Journal of
Micro/Nanolithography,
MEMS, and MOEMS

Nanolithography.SPIEDigitalLibrary.org

Electrostatically tunable MOEMS waveguide Bragg grating-based DWDM optical filter

Poorna Lakshmi Uppalapati
Balasubramanian Malayappan
Narayan Krishnaswamy
Prasant Kumar Pattnaik

SPIE.

Poorna Lakshmi Uppalapati, Balasubramanian Malayappan, Narayan Krishnaswamy, Prasant Kumar Pattnaik, “Electrostatically tunable MOEMS waveguide Bragg grating-based DWDM optical filter,” *J. Micro/Nanolith. MEMS MOEMS* **18**(1), 015503 (2019), doi: 10.1117/1.JMM.18.1.015503.

Electrostatically tunable MOEMS waveguide Bragg grating-based DWDM optical filter

Poorna Lakshmi Uppalapati,[a] Balasubramanian Malayappan,[a] Narayan Krishnaswamy,[b] and Prasant Kumar Pattnaik[a,*]
[a]Birla Institute of Technology and Science Pilani, Hyderabad Campus, Department of Electrical and Electronic Engineering, Hyderabad, Telangana, India
[b]Sai Vidya Institute of Technology, Department of Electronics and Communication Engineering, Bangalore, Karnataka, India

Abstract. An electrostatically actuated MEMS cantilever beam-based waveguide Bragg grating tunable optical filter has been designed and simulated. The tunable filter is obtained by shifting the reflected wavelength of the waveguide Bragg grating located on the electrostatically actuated cantilever beam. An approach to increasing the electrostatic actuation of the beam by having an electrode underneath the beam is used and a large wavelength tuning range for the optical filter is achieved. Dimensions of the device are chosen such that full-width-half-maximum is 0.75 nm, thus capable of filtering adjacent channels of the dense wavelength division multiplexing (DWDM) network. The filter has a tuning range of 10.65 nm (1552.52 to 1563.17 nm) providing add/drop functionality for 14 adjacent DWDM channels. *© The Authors. Published by SPIE under a Creative Commons Attribution 4.0 Unported License. Distribution or reproduction of this work in whole or in part requires full attribution of the original publication, including its DOI.* [DOI: 10.1117/1.JMM.18.1.015503]

Keywords: tunable filters; waveguide; Bragg grating; microelectromechanical systems.

Paper 18103 received Aug. 24, 2018; accepted for publication Jan. 25, 2019; published online Feb. 21, 2019.

1 Introduction

When the micromachining and electronic properties of silicon are combined with a layer of an oxide of silicon (SOI), a high refractive index contrast optically transparent medium is obtained for wavelength division multiplexing (WDM) applications. The integration of optical waveguides on a silicon substrate permits a wide variety of communication devices.[1–5] In dense WDM networks (DWDM), to carry out wavelength (channel) selection functionality, dynamic optical devices such as tunable optical filters are required. Tuning range and extinction ratio are some of the important parameters to consider while designing a tunable filter. Different optical structures have been proposed to achieve tunable filters. Silicon on insulator bandpass filters in Mach–Zehnder configuration with one arm loaded with a ring resonator has been demonstrated[6] where filter bandwidth can be tuned from 10% to 90% of free-spectral range (FSR) at an acceptable off-band rejection. However, the footprint of Mach–Zehnder interferometer (MZI)-based structures is more when compared to ring resonators and gratings. Compact ring resonators can be used as spectral filters and very narrow full-width half-maximum of 200 pm has been reported using ring resonator filters but they suffer from low tunable range through effective index variation.[7,8] Waveguide gratings as integrated filters have a footprint smaller than MZI but larger than a ring resonator. However, they are capable of being widely tuned while having frequency selectivity necessary for DWDM network. Properties of the optical filters that are commonly modified by various tuning methods are bandwidth, peak amplitude, FSR apart from peak position. Integrated tunable devices designed to tune filter bandwidth, peak amplitude, or FSR are wavelength specific and hence cannot be used to cover an entire spectrum of the optical network.

Tuning techniques in integrated optical filters can be achieved by optoelectronic and MOEMS-based techniques. The optoelectronic techniques involve methods such as ion implantation/carrier injection[9] or electro-optic[10] effect-based tuning. Due to inherent electronic nature of the tuning, these techniques have high modulation speeds. However, they suffer from a limited range of modulation or tunability. MOEMS techniques include thermo-optic,[11] acousto-optic[12] effects apart from MEMS-based electrostatic actuation[13–15] techniques. A wavelength shift of 18 nm using the thermo-optic effect[16] in Bragg grating-based silicon-on-insulator (SOI) rib waveguide loaded with the heater has been reported but has broader (4 nm) −10 dB bandwidth. This broader bandwidth cannot filter more than four channels in DWDM filter applications. The acousto-optic effect is based on a change of refractive index of a medium due to the presence of sound waves in it. Tuning techniques based on acousto-optic effect are limited by an acoustic source design and the speed of the acoustic wave. However, when combined with other components such as Bragg grating and standard diffraction mirrors, Bitauld et al.[17] have observed a very high-wavelength resolution. Using MEMS, tuning is easy and monolithic integration is possible.[18] Electrostatic actuation-based MEMS tuning is achieved through the micromachined structures such as beams, bridges, and diaphragms and by considering elasto-optic, stress-optic, and strain-optic effects. In MOEMS tuning techniques, since mechanical perturbation is involved, tuning speed is lower compared to optoelectronic ones. However, the large tuning range is obtained with MOEMS techniques. Further, multiple optical devices can be tuned simultaneously with the actuation levels depending on the physical configuration of the optical devices with respect to the MOEMS structure. In this work, we present the design of a filter with tunable

*Address all correspondence to Prasant Kumar Pattnaik, E-mail: pkpattnaik@hyderabad.bits-pilani.ac.in

peak position based on Bragg gratings with MEMS as the tuning control mechanism. This filter can be used to cover 30% of a conventional band of optical spectrum thus providing a very large tuning range.

A grating is placed on a cantilever beam such that perturbation of the beam due to electrostatic actuation causes strain along the length of the waveguide grating. Based on the work presented by Ref. 19, an integrated guided-wave MOEMS filter is designed. The above technique enables a larger tuning range of the filter. In the rest state, the designed grating has a uniform period, and under mechanical perturbation the period changes. The change in period is kept uniform by appropriate positioning of the waveguide grating on the beam. Due to the uniform change in period, the Bragg wavelength of the grating changes. With the chosen dimensions of the structure, we have obtained a tuning range of 10.65 nm with full-width-half-maximum (FWHM) of 0.75 nm which can be used to filter 14 adjacent channels in the C-band.

2 Proposed Filter Configuration

Figure 1(a) shows a schematic of the proposed electrostatically actuated MEMS cantilever beam-based waveguide Bragg grating tunable filter for C-band optical DWDM network. The cantilever beam is composed of the metal layer at the bottom, over which is a silicon dioxide beam with amorphous silicon waveguide and waveguide grating on top. The metal layer functions as the electrode for electrostatic actuation. There is an air gap between the bottom of the beam and the ground plane on the substrate. The cross-sectional view of the beam with rib waveguide grating is shown in Fig. 1(b). When the beam deflects due to electrostatic actuation, the grating period changes giving rise to shift in Bragg wavelength. As the Bragg grating acts like a filter, by varying the period, tunability can be achieved.

2.1 *Proposed Fabrication Procedure*

Fabrication of MEMS Bragg reflectors presented in the literature[18,20] generally refers to bulk micromachining of substrate to realize the MEMS device. In our design, we propose adaptation of fabrication procedures developed for plasmonic optical waveguides[21] to realize large actuation in the MEMS electrostatically actuated beam. The proposed fabrication steps are given in Fig. 2. The proposed structure can be realized by surface micromachining techniques starting with silicon wafer.[19] The silicon dioxide layer is grown by PECVD. Titanium is deposited over oxide which forms the bottom electrode. Etch and patterning of silicon dioxide and photoresist spin coat is carried out. Lithography of photoresist as a sacrificial layer is done. To achieve adhesion of metal with an oxide layer, titanium is deposited over the oxide layer by sputtering. Following this gold is electroplated to form the top electrode. Silicon dioxide and amorphous silicon layers can be deposited by PECVD on the metal layer consecutively.[21] E-beam lithography to define the beam, waveguide, and grating is carried out. The sacrificial photoresist is to be carefully chosen such that it is insensitive to developing and resist removal steps of E-beam lithography. This can be achieved by use of alkaline developer and corresponding photoresist for E-beam lithography and using SU-8 2000 as the sacrificial photoresist which can be stripped using oxidized acid solutions but not with conventional solvent-based resist strippers. The sacrificial photoresist can be stripped out to release the beam.

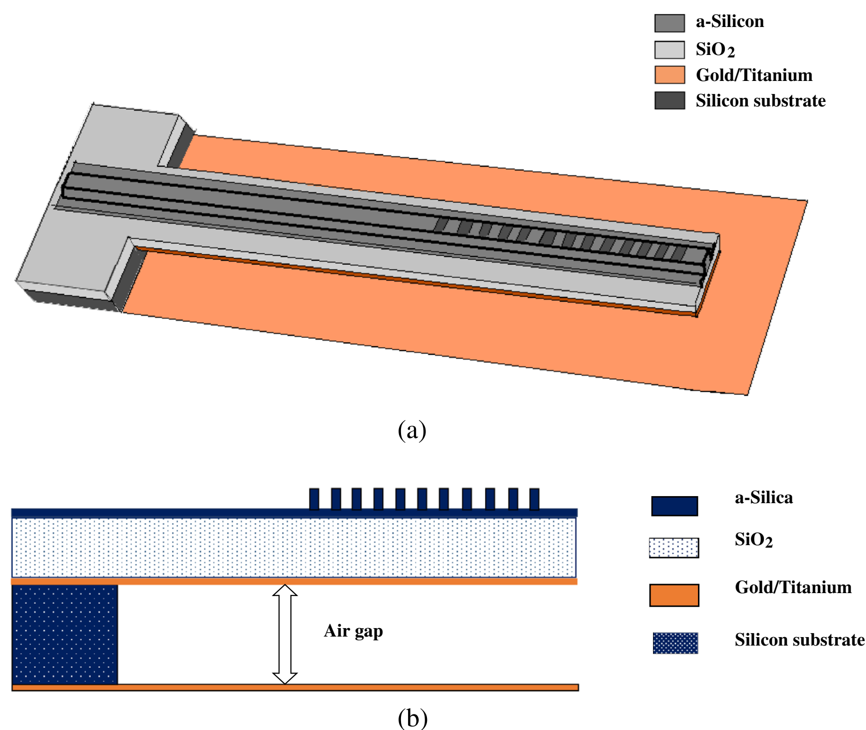

Fig. 1 (a) Schematic of the proposed device. (b) Cross sectional view of the proposed device.

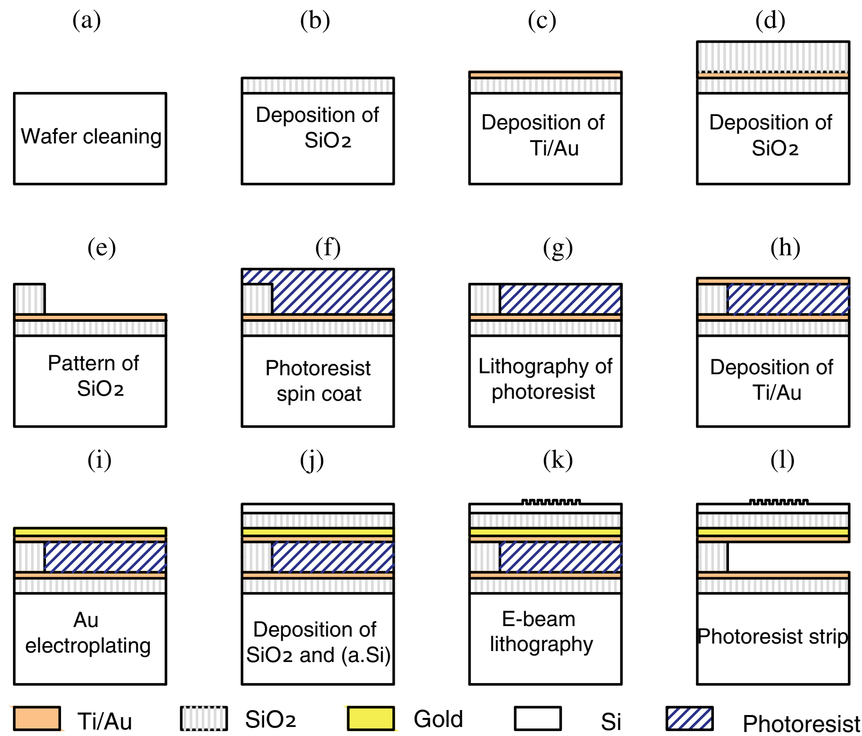

Fig. 2 (a–l) Proposed fabrication steps.

3 Design

For electrostatic actuation of MEMS beams, a ground electrode is chosen as gold. Generally, the second electrode is the topmost metal layer on the MEMS beam and its dimension determines the electric field distribution along it. The air gap and material composition of the beam apart from its dimensions determine the pull-in voltage and thus usable actuation range of the MEMS beam. As the gap between the electrodes decreases and the medium present between them has a lower dielectric constant, a better mechanical response is obtained for an applied electric potential. Thus, the electrode present underneath the MEMS beam, as shown in Fig. 1(b), maximizes the strain obtained in it. This allows the beam top surface to be used for other optical waveguides and devices. This configuration is free from plasmonic and electro-optic effects even for MEMS beams of nominal thickness.

Figure 3 shows dimensions of the proposed device. The composite MEMS cantilever beam has length 1400 μm,

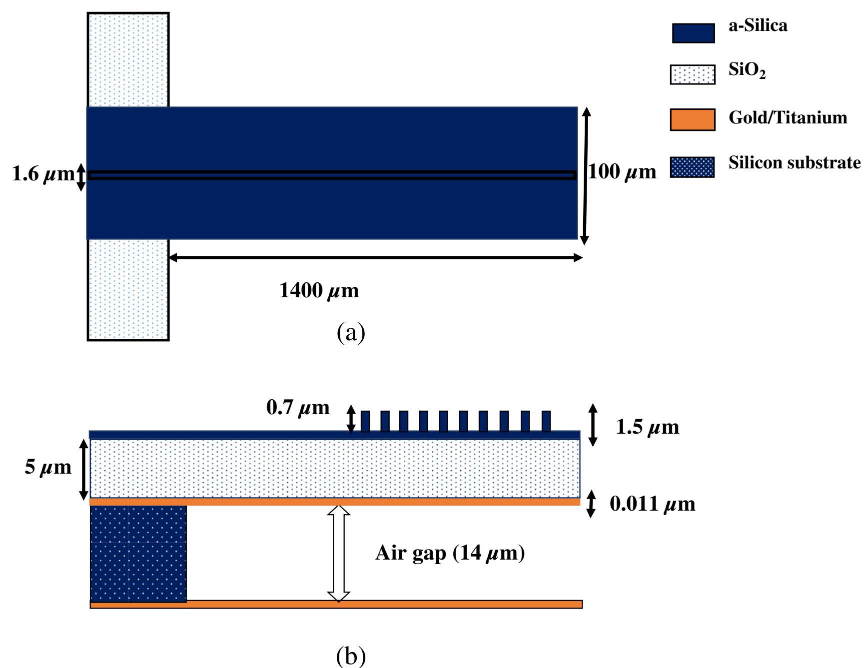

Fig. 3 Dimensions of the proposed device (a) top view (b) cross sectional view.

width 100 μm, and thickness 5.1 μm. A silicon rib waveguide of cross-section $1.5 \times 1.6\ \mu m^2$ runs along the length of the cantilever beam as shown in Fig. 3. Waveguide Bragg grating of 600 μm length is positioned at distance of 750 μm from foot of cantilever beam. The following sections detail the mechanical, optical, and optomechanical design considerations and optimization for the proposed device.

3.1 *Mechanical Design*

Tuning speed of optical filter depends on mechanical resonance of MEMS structure as the technique used for tuning is change in stress/strain of the MEMS beam in response to applied electric potential. The analysis on the design of beam parameters such as suspended beam length, the thickness of beam, the gap between ground and bottom of the beam are shown in Figs. 4–7. Figure 4 shows variation of fundamental frequency with length of the beam. The variation of resonant frequency with the length of the beam and thickness is given in Eq. (1), where l is the length of the beam, t is the thickness, E is the elastic modulus, and ρ is the density. From Eq. (1), we can see that resonant frequency is inversely proportional to length:

$$f = \frac{1}{2\pi}\sqrt{\frac{E}{\rho}\left(\frac{t}{l^2}\right)}. \tag{1}$$

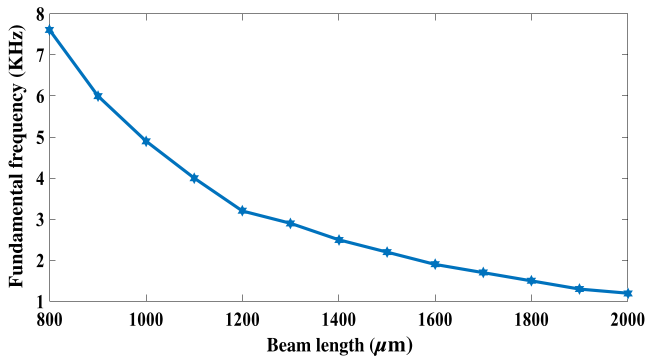

Fig. 4 Fundamental frequency variation of cantilever beam with beam length.

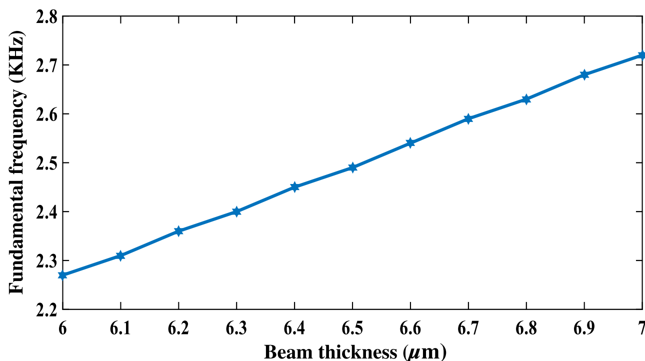

Fig. 5 Fundamental frequency variation of cantilever beam with beam thickness.

For narrow FWHM, longer length of grating is required. For appropriately placing 600 μm grating, we have chosen 1400 μm length of the beam which has fundamental frequency of 2.5 KHz under no actuation. Width of the beam is taken as 100 μm. Figure 5 shows the fundamental frequency variation with thickness of the beam. It can be seen that the increase in thickness increases the fundamental frequency as evident from Eq. (1), but strain decreases with increase in thickness as shown in Fig. 6. For this device configuration, thickness is taken as 5.1 μm. At a given voltage, strain reduces with increase in gap as shown in Fig. 7. The strain variation with increase in actuation voltage for a chosen value of 14 μm is shown in Fig. 8.

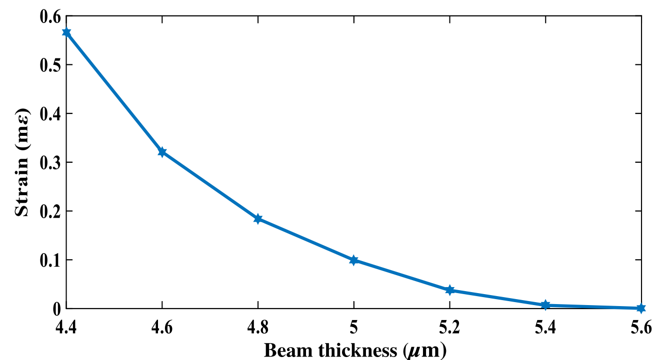

Fig. 6 Maximum value of strain with beam thickness for cantilever beam.

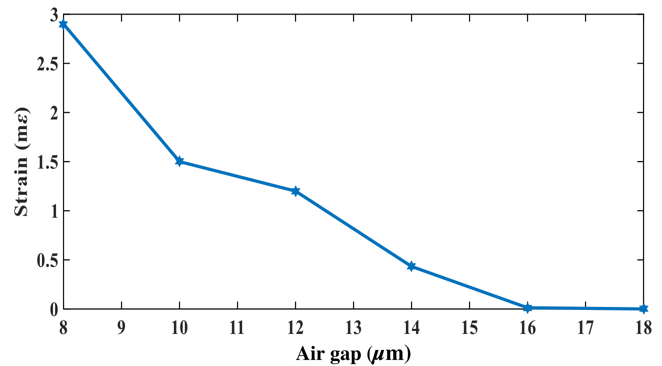

Fig. 7 Variation of maximum strain with an air gap at a given voltage of 5 V.

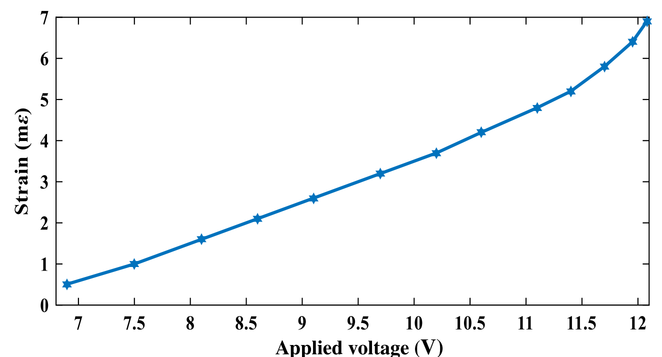

Fig. 8 Maximum strain variation for different applied voltages.

Table 1 Parameters used for pull-in voltage calculation.

Parameter	Value
E (Youngs modulus)	66.4 GPa
g_0(gap between bottom of beam and ground)	14 μm
H (thickness of beam)	5.111 μm
ν (Poisson ratio of material)	0.18
ε_0 (permittivity of free space)	8.854 pF/m
L (length of the beam)	1400 μm
W (width of the beam)	100 μm
c_1, c_2, and c_3 (constants)	0.07,1, and 0.42

The pull-in voltage of this device configuration is obtained through simulation as 12.1 V which is verified by the mathematical model as given in Eq. (2). The 100-μm wide MEMS beam is composed of silicon-dioxide of 5 μm above a gold layer of 11 nm. The a-Si is deposited and patterned in the form of a rib optical waveguide of slab height 0.8 μm and rib cross-section of 1.6×0.7 μm^2 on top of the silicon dioxide layer. The parameter values chosen to calculate the pull-in voltage of the composite beam are given in Table 1 where Young's modulus and Poisson ratio is taken as the weighted average values proportional to the individual material thickness:

$$V_{\text{pull-in}} = \sqrt{\frac{4c_1 B}{\varepsilon_0 L^4 c_2^2 \left(1 + c_3 \frac{g_0}{W}\right)}}, \tag{2}$$

where B is

$$B = \widehat{E} H^3 g_0^3. \tag{3}$$

If the beam has narrow width relative to its thickness, $\widehat{E}$ is the Young's modulus E otherwise E and $\widehat{E}$, the plate modulus are related as[22]

$$\frac{E}{\widehat{E}} = 1 - \nu^2 \left(\frac{\left(\frac{W}{L}\right)^{1.37}}{0.5 + \left(\frac{W}{L}\right)^{1.37}} \right)^{0.98\left(\frac{L}{H}\right)^{-0.056}}. \tag{4}$$

Therefore, as a trade-off, a cantilever silicon-based beam of 1400 μm length, 100 μm width, and 5.1 μm thickness with an air gap of 14 μm are considered here. The fundamental frequency of the device varies with an application of external static voltage due to a build-up of strain in the structure under steady-state conditions as shown in Fig. 9.

3.2 *Optical Design*

In this work, we have chosen a rib waveguide with a 1.5 μm thickness and 1.6 μm width. The refractive indices of the silicon dioxide and a-silicon are taken as 1.45 and 3.545 near the C-band, respectively, as shown in Fig. 10. This rib waveguide is designed to operate in a single mode at 1552.52 nm with effective refractive index of 3.49 as evident from mode profile shown in Fig. 11. The waveguide Bragg grating consists of periodic corrugations along the length of rib waveguide with a period of 222.3 nm and has a Bragg wavelength 1552.52 nm. The length of a grating is 600 μm and the modulation depth of the grating is 45 nm to obtain FWHM lower than 0.8 nm, which is desirable for C-band DWDM optical communication network with channel spacing of 100 GHz. Using finite-difference time-domain

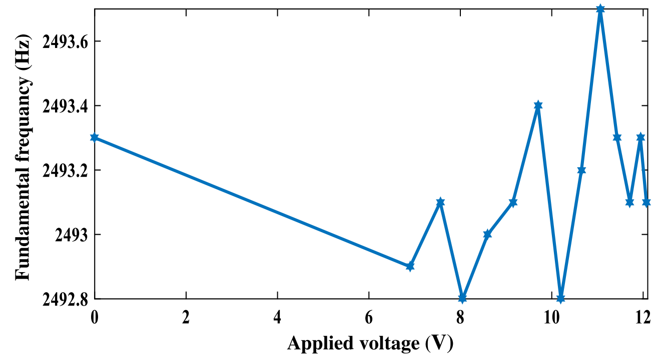

Fig. 9 Fundamental frequency variation for different applied voltages.

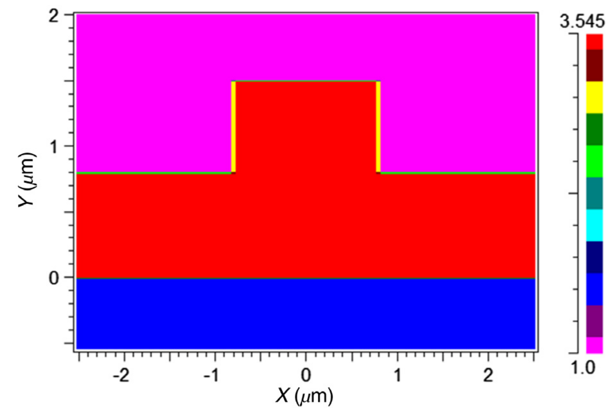

Fig. 10 Refractive index profile of rib waveguide structure.

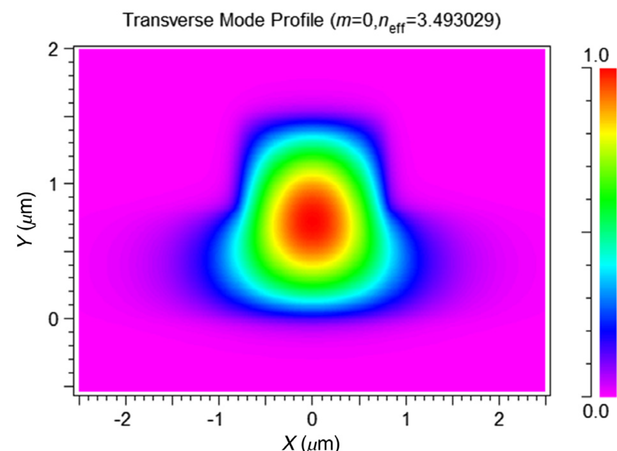

Fig. 11 Mode profile of rib waveguide.

(FDTD) simulation, the waveguide grating is found to have a propagation loss of 0.15 dB/cm.

3.3 *Optomechanical Design*

The waveguide Bragg grating is positioned along a length of the cantilever beam toward its free end. When a voltage is applied, Bragg wavelength shifts due to two effects, change in a period with strain and change in a refractive index of a waveguide with stress. In this design, the impact of strain on the optical properties of Bragg grating is more than that due to stress. As seen in Fig. 12, the peak stress occurs at the foot of the beam and remains in the order of 10^6 Pa. For silicon/SiO_2 waveguide, the corresponding stress-optic coefficients are in the order of 10^{-12} Pa^{-1}.

The period of the grating varies with voltage as given as

$$\Lambda(V) = [1 + \varepsilon(V)]\Lambda_0, \tag{5}$$

where Λ_0 is the initial period of the grating and ε is the value of strain over the grating length at a given voltage, V. It can be noted from Fig. 12 that ε varies nonuniformly along grating length thus causing chirp in the grating period. It can be noted that the strain is maximum near the free end of the beam and strain variation along beam length is minimum. Thus, the position of Bragg grating of 600 μm length is chosen as being 750 μm from the fixed end as shown in Fig. 12. For accurate analysis of the grating with nonlinear chirp, an instantaneous period of the grating is approximated to the polynomial function of fourth order which has considerably minimal error.

3.4 *Power Consumption*

Power consumption for the operation of a proposed device is observed as 0.122 nW. It has two contributing factors, the energy stored as strain in the beam and capacitive energy. Strain energy is obtained by taking line integral of strain energy density over beam length and multiplying with a cross-sectional area since the beam has a uniform cross-section. Variation of strain energy density over a length at a voltage of 12.07 V is shown in Fig. 13 and the maximum strain energy obtained is 1.8 pJ. In the proposed structure, the two electrodes and the gap between them form a capacitor.

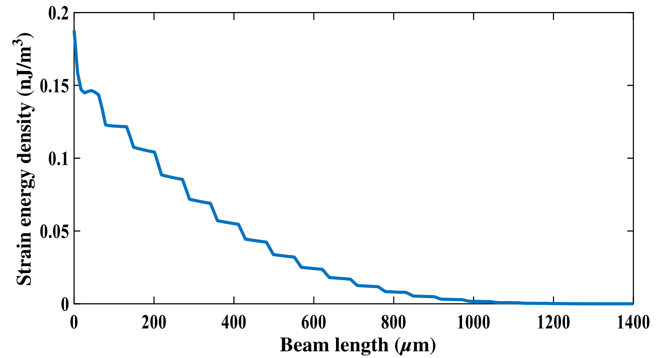

Fig. 13 Strain energy density of the device at 12.07 V applied voltage.

Capacitive energy, the energy required to maintain the potential difference across these electrodes, is 0.12 nJ at the maximum voltage of 12.07 V. Thus maximum power consumption for the proposed structure is estimated as 0.122 nW.

4 Simulation and Results

The mechanical characteristics of the cantilever beam were studied numerically using finite element analysis and optical characteristics of waveguide grating were analyzed numerically using coupled mode theory. The Bragg wavelength for unperturbed grating with period 222.3 nm at no actuation is 1552.52 nm with the FWHM of 0.75 nm which is less than 0.8 nm required for DWDM optical network. When the cantilever beam is actuated electrostatically with 12.07 V applied voltage the Bragg wavelength shifts to 1563.17 nm as observed from Fig. 14, thus providing a total tuning range of 10.65 nm. By careful design, optimization minor effects that affect device performance can be minimized. Temperature invariance along length can be achieved by appropriate positioning of the electrode contact pads, which is the major cause of heating/temperature variation. The waveguide and grating carrying DWDM optical signal is on the top surface of the largely insulating (SiO_2) beam of 5.1 μm thickness. And the electric potential is applied to the bottom of the beam. Thus, the optical medium is insulated from electrostatic field edge effect.

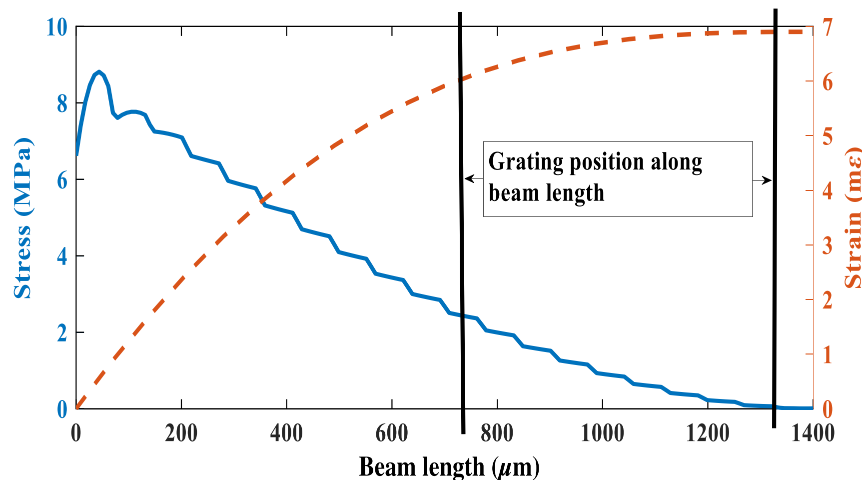

Fig. 12 Stress and strain along the beam length at 12.07 V.

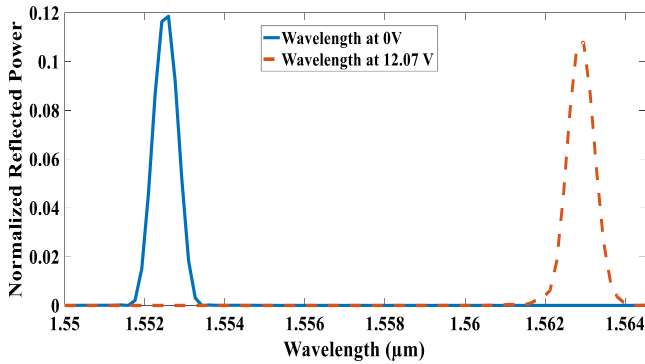

Fig. 14 Bragg wavelength shift at 12.07 V applied voltage.

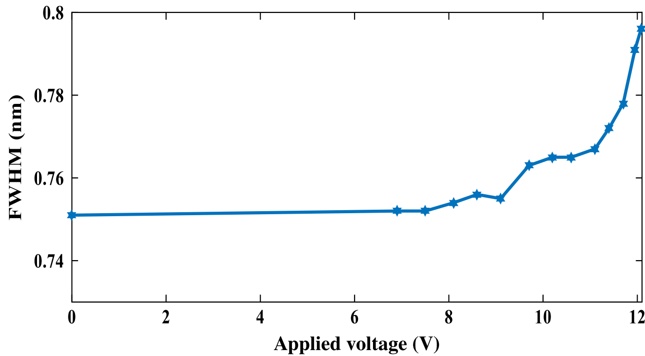

Fig. 15 FWHM of reflected spectrum over the tuning range.

Figure 15 shows variation of FWHM with applied voltages up to pull-in value. It can be seen from Fig. 15 that FWHM lies below 0.8 nm for all the voltages. By applying different voltages to the cantilever beam, the Bragg wavelength shifts and hence we can achieve a tunable filter. Table 2 shows the Bragg wavelength for various applied voltages from 0 to 12.07 V. The maximum voltage that can be applied for the cantilever beam is limited by pull-in voltage which is 12.1 V for chosen parameters. From Table 2, we can observe that 14 DWDM channels (1552.52 to 1563.17 nm) can be tuned by applying 0 to 12.07 V and the maximum peak position deviation is not greater than 0.04 nm at the given applied voltages. Figure 16 shows the reflected Bragg wavelength with applied voltages from 6.9 to 12.07 V. This variation can be put in a cubic polynomial fit as Eq. (6), where λ is the wavelength in nm and V is the voltage in volts:

$$\lambda(V) = 0.0041039V^3 + 0.51784V^2 - 0.40089V + 1552.5. \tag{6}$$

It can be observed that for the applied voltage range of 6.9 to 10.65 V the Bragg wavelength shifts from 1553.32 to 1558.92 nm is linear with a sensitivity of 0.17 nm/V. Also for the applied voltage range of 11.06 to 11.71, the Bragg wavelength shifts from 1559.71 to 1561.31 nm with a sensitivity of 0.1 nm/V. Further, we note that for the applied voltages from 11.94 to 12.07 V Bragg wavelengths shifts from 1562.15 to 1562.90 nm with voltage sensitivity of a 0.04 nm/V. Care must be taken when the voltage

Table 2 Bragg wavelength variation with applied voltage.

Channel number	Actuation voltage (V)	Reflected wavelength (nm)	ITU-T standard wavelength (nm)	Deviation (nm)
1	0	1552.52	1552.52	0.00
2	6.9	1553.32	1553.32	0.00
3	7.56	1554.16	1554.12	0.04
4	8.05	1554.90	1554.92	0.02
5	8.6	1555.72	1555.72	0.00
6	9.15	1556.53	1556.52	0.01
7	9.7	1557.36	1557.32	0.04
8	10.2	1558.15	1558.12	0.03
9	10.65	1558.92	1558.92	0.00
10	11.06	1559.71	1559.72	0.01
11	11.43	1560.54	1560.52	0.02
12	11.71	1561.31	1561.32	0.01
13	11.94	1562.15	1562.12	0.03
14	12.07	1562.90	1562.92	0.02

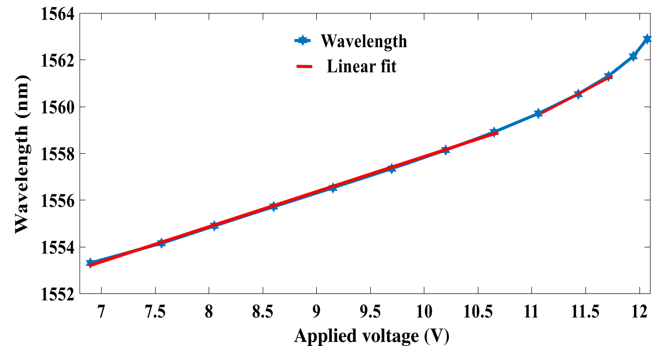

Fig. 16 Bragg wavelength with applied voltage.

is approaching close to the device pull-in voltage of 12.1 V. Table 3 shows the voltage tolerance range for reliable operation of proposed C-band 100 GHz DWDM optical filter for a wavelength range of 1553.32 to 1561.31 nm. Here, we have considered the allowed deviation of Bragg peak position to be below 0.25 nm for optimal performance. For channels 2 to 9 where voltage tuning sensitivity is 1.49 nm/V, 0.17 V applied voltage can be tolerated in each channel. For channels 10 to 12 where the tuning sensitivity of 2.46 nm/V, 0.1 V applied voltage can be tolerated. Similarly, for channels 13 to 14 where the tuning sensitivity of 5.76 nm/V, 0.04 V applied voltage can be tolerated.

Table 3 Voltage tolerance range for DWDM channels.

Channel number	DWDM wavelength (nm)	Tolerance (V)	Voltage range (V)
2	1553.32	0.17	6.73 to 7.07
3	1554.162	0.17	7.39 to 7.73
4	1554.92	0.17	7.88 to 8.22
5	1555.72	0.17	8.43 to 8.77
6	1556.53	0.17	8.98 to 9.32
7	1557.36	0.17	9.53 to 9.87
8	1558.12	0.17	10.03 to 10.37
9	1558.92	0.17	10.48 to 10.82
10	1559.71	0.1	10.96 to 11.16
11	1560.54	0.1	11.33 to 11.53
12	1561.31	0.1	11.61 to 11.81

5 Conclusions

An electrostatically actuated MEMS cantilever beam-based waveguide Bragg grating tunable optical filter has been presented in this work. An approach to increasing the electrostatic actuation of the beam by having an electrode underneath the beam is used and a large wavelength tuning range for the optical filter is achieved. A narrow FWHM of 0.75 nm was achieved for the chosen dimensions of this device allowing filtering of adjacent channels of DWDM network, separated by 0.8 nm. The filter can be tuned from 1552.52 to 1563.17 nm (14 DWDM channels) utilizing look-up Table 2. The tuning behavior is linear in the wavelength regions 1553.32 to 1558.92 nm, and 1559.71 to 1561.31 nm with tuning voltage sensitivities of 0.17 and 0.1 nm/V, respectively. All the channels from 1 to 14 (1552.52 to 1562.90 nm) can be filtered out with the applied voltages given in Table 2. Taking into account voltage tolerance of actuation, pull-in voltage, and frequency stability of the beam, the filter has a tuning range of 10.65 nm (1552.52 to 1563.17 nm) providing add/drop functionality for 14 adjacent DWDM channels.

Acknowledgments

One of the authors, Prasant Kumar Pattnaik, would like to thank BITS Pilani for supporting this work through Grant No. BITS/OPERA/475.

References

1. D. T. Neilson et al., "Wavelength selective switching for optical bandwidth management," *Bell Labs Tech. J.* **11**, 105–128 (2006).
2. N. Kobayashi et al., "Silicon photonic hybrid ring-filter external cavity wavelength tunable lasers," *J. Lightwave Technol.* **33**(6), 1241–1246 (2015).
3. H. Ma et al., "Tilted waveguide gratings and implications for optical waveguide-ring resonator," *J. Lightwave Technol.* **33**(19), 4176–4183 (2015).
4. R. D. Mansoor et al., "Estimation of the bandwidth of acceptable crosstalk of parallel coupled ring resonator add/drop filters," *IEEE Trans. Electromagn. Compat.* **57**(5), 1005–1012 (2015).
5. P. Orlandi et al., "Tunable silicon photonics directional coupler driven by a transverse temperature gradient," *Opt. Lett.* **38**(6), 863–865 (2013).
6. P. Orlandi et al., "Tunable bandwidth optical filter in SOI," in *Eur. Conf. Integr. Opt. (ECIO)*, pp. 1–2 (2012).
7. W. Bogaerts et al., "Silicon microring resonators," *Laser Photonics Rev.* **6**(1), 47–73 (2012).
8. R. Marchetti et al., "Low-loss micro-resonator filters fabricated in silicon by CMOS-compatible lithographic techniques: design and characterization," *Appl. Sci.* **7**(2), 174 (2017).
9. Q. Fang et al., "Carrier-induced silicon waveguide Bragg grating filter based on ion implantation," in *Opt. Fiber Commun. Conf.*, Optical Society of America, OTu3C–8 (2013).
10. J. Takayesu et al., "A hybrid electrooptic microring resonator-based 1×4×1ROADM for wafer scale optical interconnects," *J. Lightwave Technol.* **27**(4), 440–448 (2009).
11. V. M. Passaro, A. V. Tsarev, and F. De Leonardis, "Wavelength interrogator for optical sensors based on a novel thermo-optic tunable filter in SOI," *J. Lightwave Technol.* **30**(13), 2143–2150 (2012).
12. A. Tsarev and E. Kolosovsky, "New architecture of tunable acoustooptical add/drop multiplexer for dynamic DWDM with 25 GHz ITU grid," in *IEEE Ultrason. Symp.*, Vol. 1, pp. 64–67 (2004).
13. M. C. Wu, O. Solgaard, and J. E. Ford, "Optical MEMS for lightwave communication," *J. Lightwave Technol.* **24**(12), 4433–4454 (2006).
14. T. Venkateshkanna and K. Wilson, "Application of optical-MEMS in lightwave communications," in *IEEE Int. Conf. Emerging Trends Electr. Eng. and Energy Manage. (ICETEEEM)*, pp. 455–464 (2012).
15. L. Y. Lin and E. L. Goldstein, "Opportunities and challenges for MEMS in lightwave communications," *IEEE J. Sel. Top. Quantum Electron.* **8**(1), 163–172 (2002).
16. S. Honda et al., "Largely-tunable wideband Bragg gratings fabricated on SOI rib waveguides employed by deep-RIE," *Electron. Lett.* **43**(11), 630–631 (2007).
17. D. Bitauld et al., "A fast tunable high resolution filter," in *IEEE Conf. Lasers and Electro-Opt. Eur., CLEO/Europe*, p. 498 (2005).
18. K. Reck, E. V. Thomsen, and O. Hansen, "All-optical frequency modulated high pressure MEMS sensor for remote and distributed sensing," *Sensors* **11**(11), 10615–10623 (2011).
19. S. Kafumbe et al., "Operational process for manufacturing a MEMS micro-cantilever system," in *Int. Conf. Ind. Eng. and Oper. Manage. (IEOM)*, IEEE, pp. 1–7 (2015).
20. K. Reck, E. V. Thomsen, and O. Hansen, "MEMS Bragg grating force sensor," *Opt. Express* **19**(20), 19190–19198 (2011).
21. F. Lou, "Design, fabrication and characterization of plasmonic components based on silicon nanowire platform," PhD Thesis, KTH Royal Institute of Technology (2014).
22. R. K. Gupta et al., "Electrostatic pull-in test structure design for in-situ mechanical property measurements of microelectromechanical systems (MEMS)," PhD Thesis, Massachusetts Institute of Technology (1997).

Poorna Lakshmi Uppalapati is pursuing her PhD in photonics at BITS Pilani, Hyderabad campus. She received her MTech degree in communications in 2011. She was associated with academics as an assistant professor during the period 2003 to 2009 and from 2011 to 2013. Her research interest is tunable devices for optical communication networks. She is a member of IEEE and IEEE Photonics Society.

Balasubramanian Malayappan received his BE (Hons) degree in electronics and instrumentation engineering and master's degree in communication engineering in 2010 and 2013, respectively, from BITS-Pilani, Pilani campus, India. He is pursuing his doctoral degree in optical MEMS at BITS Pilani, Hyderabad campus, where he is also a lecturer in the Department of Electrical Engineering. He is a student member of IEEE and IEEE Photonics Society.

Narayan Krishnaswamy received a doctorate from Indian Institute of Science Bangalore in 2012. His doctoral research was inter-disciplinary; he was associated with Department ECE, Department of Instrumentation, and Centre for Nano Science and Engineering at IISc, Bangalore. He has a BE degree in electrical and electronics engineering from VTU, Belgaum, India, and an MTech degree in biomedical engineering from Manipal University, India. He is presently

executing sponsored research projects from DST-SERB, Govt. of India and VGST, Department of IT and BT, Govt. of Karnataka.

Prasant Kumat Pattnaik is an assistant professor in the Department of Electrical and Electronic Engineering at BITS Pilani Hyderabad Campus, India. He received his PhD in electrical communication engineering from Indian Institute of Science, Bangalore, India, in 2005. Prior to joining BITS, he has worked as a specialist in design and development at Tata Elxsi Ltd., Bangalore, and as a postdoctoral research associate at IISc Bangalore. His main research interests are in photonic integrated circuits, optical communication, MEMS and MOEMS, and photonic devices for sensors and communication. He has published about 50 papers in international journals and conferences.